European Journal of Mechanics / A Solids 104 (2024) 105162

Contents lists available at ScienceDirect

European Journal of Mechanics / A Solids

journal homepage: www.elsevier.com/locate/ejmsol

Adiabatic limit for scattering-free waveguiding in space-graded arrays of micro-resonators

E. Riva [a], J.M. De Ponti [b], J. Marconi [a], F. Braghin [a], R. Ardito [b], A. Corigliano [b,*]

[a] Department of Mechanical Engineering, Politecnico di Milano, Via La Masa 1, 20156, Milano, Italy
[b] Department of Civil and Environmental Engineering, Politecnico di Milano, Piazza Leonardo da Vinci 32, 20133, Milano, Italy

ARTICLE INFO

Keywords:
Rainbow effect
Graded metamaterials
Adiabatic theorem
Phononic crystals
Elastic waveguides

ABSTRACT

We report on the dynamics of graded metamaterials in the context of micro-electromechanical systems (MEMS). Graded metamaterials are known to exhibit space confinement of mechanical energy - or *rainbow trapping* - in response to a tailored wave speed reduction. Such a behavior, in turn, is controlled by a gradual variation of the resonant characteristics of an array of resonators dressed on a host structure which, as a result, exhibits arbitrarily slow waves. The paper shows quantitatively that there is an adiabatic limit for the rate of change of the grading. Below this limit, the rainbow effect takes place with a negligible scattering of energy, which is otherwise detrimental to practical applications such as harvesting, sensing, and communication. The paper also paves new ways to manipulate wave motion in MEMS through elastic metamaterials.

1. Introduction

By dressing elastic metamaterials onto host structures, a number of unusual functionalities, inherently linked to different forms of periodic, quasiperiodic, and aperiodic tessellations, can be activated. In other words, one can take advantage of geometrical degrees of freedom to mold architected systems with unusual characteristics in reciprocal space, which manifest themselves in physical space through states with nontrivial topological signature (Moore, 2010; Mousavi et al., 2015; Huber, 2016; Deng et al., 2022; Miniaci et al., 2018; Riva et al., 2018; Wang et al., 2015; De Ponti et al., 2023), nonreciprocal waves (Marconi et al., 2020; Palermo et al., 2020), and wave steering capabilities (Colombi et al., 2016b; Yan and Gao, 2023; Tol et al., 2017), to name a few. The underlying idea is to tailor specific tessellations, capable of taming waves through effective dynamical properties (Antonakakis et al., 2013; Sridhar et al., 2016) impossible to observe in homogeneous materials, whereby applications at different scale levels can benefit these new dynamical characteristics and meet otherwise non-accessible technological needs.

Whilst most examples usually exhibit fixed (non-varying) dispersion in physical space, a recent line of work leverages the gradual modulation of one or more relevant parameters to slow down or speed-up wave motion (De Ponti et al., 2019; De Ponti, 2021; Chaplain et al., 2020a; Zhao et al., 2022). This phenomenon – also known as the *rainbow effect* (Tsakmakidis et al., 2007) – has been investigated through different physical platforms and has led to experimental works that have propelled the research done in the context of graded metamaterials (De Ponti et al., 2020, 2021b; Alshaqaq et al., 2022; Chaplain et al., 2020a,c). The key idea is to take advantage of resonator-structure interactions to induce a frequency-invariant wavenumber transformation dictated by the gradual variation of the resonance frequency in space.

A notable example extensively discussed in the literature consists of a graded array of resonators rigidly connected atop an elastic half-space. Such a configuration is known to exhibit the rainbow effect, whereby the wave, initially accelerated when confined to the boundary, is mode-converted from being localized as a surface wave to a shear/pressure wave propagating in the bulk of the material (Colombi et al., 2016a; Chaplain et al., 2020b; Palermo et al., 2016; Alan et al., 2019). Other forms of graded metamaterials include 1D waveguides that support a trapping mechanism suitable to confine energy in space and, hence, convenient for harvesting purposes, e.g. in autonomous sensors (De Ponti, 2022). We note that the achievable functionalities of graded materials are not limited to the aforementioned examples but include a number of rich wave phenomena emerging from a slow modulation of one or more parameters, such as flexural-to-torsional mode-conversion (De Ponti et al., 2021a), spatial frequency separation (Santini et al., 2022), and adiabatic pumping (Riva et al., 2020; Xia et al., 2021; Grinberg et al., 2020).

It is therefore important to study the conditions under which the rainbow effect manifests in spatially varying metamaterials and to understand how the choice of the graded profile influences the underlying

* Corresponding author.
E-mail address: alberto.corigliano@polimi.it (A. Corigliano).

https://doi.org/10.1016/j.euromechsol.2023.105162
Received 3 February 2023; Received in revised form 1 September 2023; Accepted 14 October 2023
Available online 20 October 2023

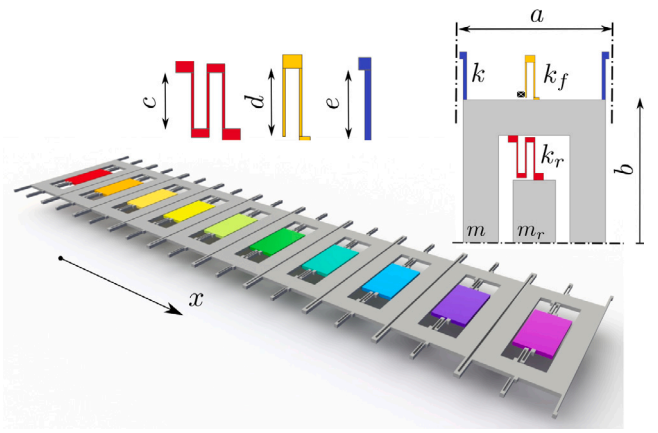

Fig. 1. Graphical representation of the MEMS spring–mass chain with local resonators. The system includes a number of masses (external frame) equipped with resonating masses (colored solids). The ligaments are used as elastic elements to connect host masses and resonating masses (k_r), consecutive host masses (k), and host masses to ground (k_f). The colors illustrate that there is a variation of the resonating mass along x. (For interpretation of the references to color in this figure legend, the reader is referred to the web version of this article.)

dynamics. Motivated by this, the paper delineates the limiting parameters for a modulation to be considered adiabatic and, hence, suitable to produce slow waves. In analogy with the temporal counterpart (Santini and Riva, 2023), the problem is addressed via the adiabatic theorem, whereby the energy, initially stored in a target mode, is assumed to leak during nonadiabatic variation of the resonance frequency in space. The velocity of the transformation is linked to the energy scattering between the wave modes supported by the waveguide, providing a machinery to quantify the degree of adiabaticity of the transformation. Practically, nonadiabatic gradings can generate reflected waves that (i) reduce the energy that can be potentially trapped, and (ii) alter the wave field within the material, which is undesired for signal processing and communication purposes. The above aspects are explored in our paper and hereafter applied to a MEMS spring–mass chain where, for simplicity, the resonating mass is varied in space. Our paper also attempts to bridge the gap between recently explored behaviors at the macroscale and the physics of metamaterials in microsystems, where the contribution is limited to a few yet very promising applications (Cha et al., 2018; Dubček et al., 2021; Marconi et al., 2023).

The paper is organized as follows. Section 2 discusses the simplified and full-order models employed to perform numerical simulations. A quantitative condition, which delineates the transition between adiabatic and nonadiabatic grading, is presented in Section 3. In Section 4 the numerical results are reported and discussed critically, with particular emphasis on the role of the grading steepness on the rainbow effect. Concluding remarks are reported in Section 5.

2. Modeling: from MEMS resonators to homogenized continuum

Consider the graded metamaterial illustrated in Fig. 1 and hereafter studied by means of three visually different yet dynamically equivalent models, all representing a MEMS spring–mass chain. The latter features a planar geometry that is dictated by the MEMS production process (Deep Reactive Ion Etching, DRIE), consisting of the etching of a plane silicon wafer by means of a plasma jet. In this context, springs are usually designed as flexible folded beams (Corigliano et al., 2017), as shown in the inset of Fig. 1. The system is thus tailored to operate at the micro-scale and, for simulation purposes, obeys the elastodynamic equations of a solid under plane stress conditions. Such a system can be represented through an elastic lattice (Fig. 2(a)), where each mass is regarded as a rigid element. In the low-frequency regime, the elastic lattice can be homogenized to resemble a rod as shown in Fig. 2(b). This form is more functional to illustrate the role of grading in the formation of slow waves. To emulate the rainbow effect, a linear distribution of resonating masses (represented with colors) is hereafter applied to gradually modify the wavenumber content of the impinging wave, which is accompanied by a wave speed variable in space.

We start the discussion from Fig. 1, whereby a number of elements with mass $m = 116.5$ ng are equally spaced by a lattice constant $a = 205$ μm and grounded by way of stiffness elements $k_f = 94.79$ N/m. As it will be shown, the ground spring is used to obtain a self-sustained structure and has a relatively low impact on the dispersion relation in the region of interest. Each element is connected to nearest neighbors through linear elastic springs $k = 772.2$ N/m and equipped with a resonating element characterized by resonance frequency $\omega_r = \sqrt{k_r/m_r}$ where $k_r = 88.8$ N/m and m_r are the resonator stiffness and mass, being this latter variable along x to induce the rainbow effect. Note that the values for k_f, k, and k_r are inherently linked to the geometrical parameters of the spring and evaluated through a static finite element analysis. For completeness, we report the relevant values for the beam lengths $b = 200$ μm, $c = 42.9$ μm $d = 49.1$ μm and $e = 57$ μm, and respective widths $w_c = w_d = 2$ μm and $w_e = 5$ μm. Hence, a lumped parameter model for such a system can be easily deduced and represented schematically as done in Fig. 2(a), where $u^{(n)}$ and $u_r^{(n)}$ are the longitudinal motion of the mass element along the chain and the longitudinal motion of the resonator, respectively.

First and foremost, we provide the equation of motion for such a system, where each element is considered as a lumped element to ease numerical simulations. Later, we consider a homogenized version, which is more suitable to address adiabaticity (Santini and Riva, 2023). Both models will be validated through COMSOL Multiphysics by way of a finite element discretization of the system shown in Fig. 1(a).

The elastodynamic equation of motion for the lattice model in Fig. 2(a) reads:

$$\begin{aligned} &m\ddot{u}^{(n)} + \left(2k + k_f\right) u^{(n)} + k_r \left(u^{(n)} - u_r^{(n)}\right) - k(u^{(n-1)} + u^{(n+1)}) = 0 \\ &m_r \ddot{u}_r^{(n)} + k_r \left(u_r^{(n)} - u^{(n)}\right) = 0. \end{aligned} \tag{1}$$

$u^{(n)}$ are sought in exponential form $u^{(n)} = \hat{u}^{(n)}\, \mathrm{e}^{j(n\mu - \omega t)}$, where ω and $\mu = \kappa a$ are frequency and dimensionless wavenumber, respectively. Plugging $u^{(n)}$ in the governing Eq. (1) gives the following dispersion relation:

$$\cos\mu = \frac{1}{2}\left(2 + \gamma_f + \gamma_r - \frac{\omega^2}{\omega_0^2} - \frac{\gamma_r}{1 - \frac{\omega^2}{\omega_r^2}}\right), \tag{2}$$

where $\omega_0 = \sqrt{k/m}$. Here, dimensionless quantities $\gamma_f = k_f/k$ and $\gamma_r = k_r/k$ are introduced.

A different approximation for the dispersion relation is achieved from the homogenized version of the lattice (Fig. 2(b)). As such, the governing equation is deduced by assuming continuous quantities for the ground spring and the resonating elements, as well as for the linear elasticity between nearest neighbors. Moreover, the effective mass is adopted (Milton and Willis, 2007):

$$m_{eff} = m + \frac{m_r}{1 - \frac{\omega^2}{\omega_r(x)^2}}, \tag{3}$$

The homogenized governing equation reads:

$$\frac{\partial}{\partial x}\left(ka\frac{\partial u}{\partial x}\right) - \frac{k_f}{a}u = \frac{m_{eff}}{a}\frac{\partial^2 u}{\partial t^2}. \tag{4}$$

The solution is sought in the form $u(x,t) = \hat{u}\mathrm{e}^{j\left(\frac{\mu x}{a} - \omega t\right)}$, yielding the dispersion relation:

$$\mu^2 = -\frac{k_f}{k} + \omega^2 \frac{m_{eff}}{k} \tag{5}$$

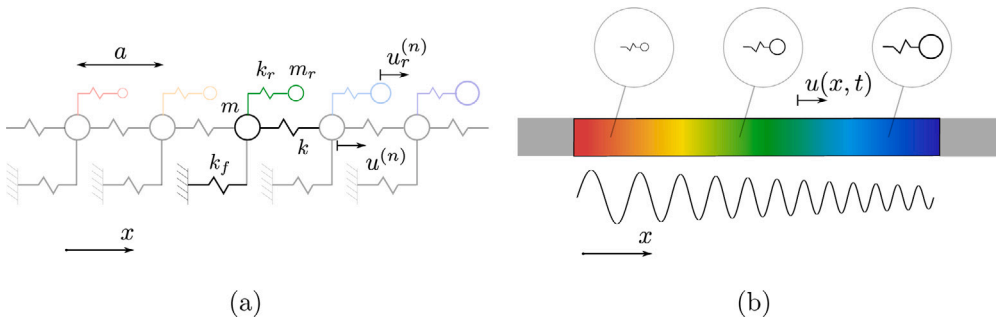

Fig. 2. (a) Lattice approximation for the MEMS device. (b) Schematic of the homogenized version of the system, whereby the color is representative of a continuous modulation of the resonating mass in space. The figure shows also schematically that there is a wavenumber transformation in response to the grading.

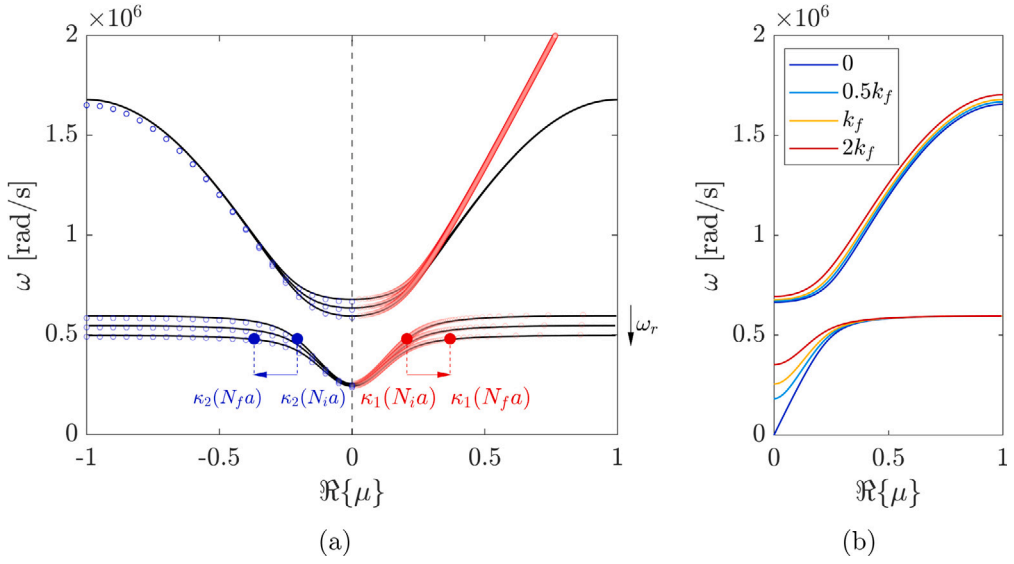

Fig. 3. (a) Dispersion relation for three different values of resonating mass. The black line is relative to the lattice model, while the red dots are obtained through the homogenized model. The dispersion curves are also validated through COMSOL Multiphysics (blue dots). (b) Effect of ground spring variation with respect to the nominal value (k_f). (For interpretation of the references to color in this figure legend, the reader is referred to the web version of this article.)

After the introduction of the definition of the effective mass, Eq. (3), one finds:

$$\mu^2 = -\gamma_f + \omega^2 \left(\frac{1}{\omega_0^2} + \frac{\gamma_r/\omega_r^2}{1 - \frac{\omega^2}{\omega_r^2}} \right). \tag{6}$$

As a matter of fact, the dispersion relation in Eq. (6) can be obtained from Eq. (2) as the limit case when $a \to 0$, that means $\mu \to 0$.

The dispersion relations for the above models and for the finite element solution synthesized in COMSOL Multiphysics are compared in Fig. 3(a). The black lines are evaluated through the lattice model, while the homogenized dispersion is illustrated by way of red dots and, finally, the COMSOL model is displayed with blue dots. All models are in good agreement, especially in the neighborhood of the gap, where the homogenization limit is satisfied. To ease visualization, three representative dispersion relations are displayed, which correspond to arrays with fixed ω_r values equal to the starting $\omega_{r,i}$, intermediate $\omega_{r,m}$, and final $\omega_{r,f}$ values of the grading. We can conclude that all the models are representative of the same underlying dynamics. Finally, the dispersion relation upon varying k_f is reported in Fig. 3(b). The analysis shows that k_f has a large influence only at low frequencies, while the effect close to resonance is limited.

3. Adiabatic limit for a space-graded array of resonators

At this step, it is expected that the rainbow effect manifests if the resonance frequency $\omega_r = \omega_{r,i} - v_m \left(x - N_i a \right)$ is varied from $\omega_{r,i}$, to $\omega_{r,f}$, whereby a frequency-preserving wavenumber transformation $\kappa_1 \left(N_i a \right) \to \kappa_2 \left(N_f a \right)$ takes place along space from $x = N_i a$ to $x = N_f a$ and is accompanied by a wave speed decrease. Here, v_m is the steepness of the grading, $N_i a$ and $N_f a$ are the initial and final positions, and N_i, N_i are the corresponding mass indices. Such a transformation, occurring at the excitation frequency ω and in case of a positive traveling wave (positive wavenumber), is represented with red dots and arrows in Fig. 3(a). Note that, if the transformation occurs adiabatically, wave propagation occurs without energy scattering toward other states populating the lattice at the same excitation frequency and for different wavenumbers. In the case at hand, there is only one additional state at negative wavenumbers, which is represented with the blue dots and arrows in Fig. 3(a) and constitutes a back-propagating wave. This aspect is hereafter unfolded and discussed by starting from the governing Eq. (4) with implied frequency dependence and suitably combined with the adiabatic theorem to shed light on the role of the modulation velocity.

Eq. (4) is recast as a system of first-order differential equations in matrix form:

$$|\Psi_{,x}\rangle = H(x,\omega)\,|\Psi\rangle \qquad |\Psi\rangle = \begin{pmatrix} \partial u/\partial x \\ u \end{pmatrix}$$
$$H(x,\omega) = \begin{bmatrix} 0 & \frac{-k_f + m_{eff}(x)\omega^2}{ka^2} \\ 1 & 0 \end{bmatrix}, \tag{7}$$

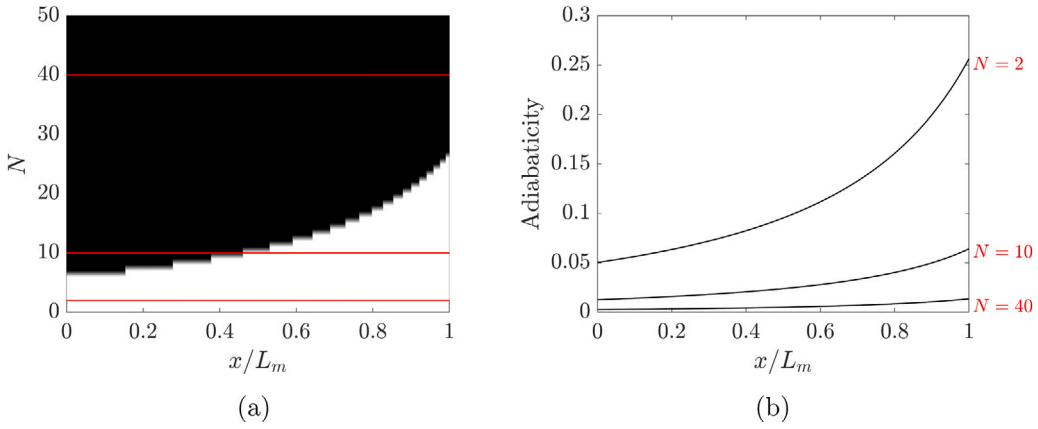

Fig. 4. (a) Adiabatic limit separating the region where the graded metamaterial is adiabatic (black domain) and nonadiabatic (white domain). The border is defined by exploring the region of space included within the grading, and upon varying the number of unit elements N. The three values for N employed in the simulation are marked in red and also used in (b) to illustrate degree of adiabaticity obtained through Eq. (10).

where an impinging wave with frequency ω is considered. Here, $(.)_{,x}$ stands for $\partial(.)/\partial x$ and $m_{eff}(x)$ is the effective dynamic mass density, which is variable with x due to the implied grading law for ω_r. Ansatz in the form $|\boldsymbol{\Psi}\rangle = |\boldsymbol{\psi}_n\rangle e^{j\kappa x}$ effectively describe an eigenvalue problem $H(x,\omega)\,|\boldsymbol{\psi}_n^R\rangle = j\kappa_n |\boldsymbol{\psi}_n^R\rangle$ equivalent to the dispersion relation in Eq. (6). The formulation highlights that, for a given impinging frequency ω, a pair of states with opposite wavenumbers $\kappa_{1,2} = \pm\kappa$ populate the lattice, corresponding to counter-propagating waves. To ease interpretation, the two states and their evolution in space are marked with blue/red dots and arrows in Fig. 3(a). The analogy with time-dependent lattices (Santini and Riva, 2023; Riva et al., 2021) suggests that the energy, initially injected in $\kappa_1 = -\kappa$ (i.e., a wave propagating from left to right), does not leak to $\kappa_2 = \kappa$ (i.e. from right to left) if a sufficiently slow - or adiabatic-modulation is considered. The degree of adiabaticity is quantified by adapting the adiabatic theorem to make it applicable to space metagradings (Santini and Riva, 2023; Riva et al., 2021):

$$\left| \frac{\left\langle \boldsymbol{\psi}_2^L \right| H(x,\omega)_{,x} \left| \boldsymbol{\psi}_1^R \right\rangle}{\left(\kappa_2 - \kappa_1\right)^2} \right| \ll 1, \tag{8}$$

where $|\boldsymbol{\psi}_1^R\rangle$ and $\langle\boldsymbol{\psi}_2^L|$ are the left and right eigenvectors relative to $\kappa_{1,2} = \pm\kappa$ and suitably normalized such that $\left\langle \boldsymbol{\psi}_i^L \middle| \boldsymbol{\psi}_j^R \right\rangle = \delta_{ij}$:

$$\begin{aligned} \left|\boldsymbol{\psi}_1^R\right\rangle &= \begin{pmatrix} \frac{j}{\sqrt{2}}\sqrt{\frac{m_{eff}\omega^2 - k_f}{ka^2}} \\ \frac{1}{\sqrt{2}} \end{pmatrix} & \left\langle \boldsymbol{\psi}_1^L \right| &= \begin{pmatrix} \frac{1}{j\sqrt{2}}\sqrt{\frac{ka^2}{m_{eff}\omega^2 - k_f}} & \frac{1}{\sqrt{2}} \end{pmatrix} \\ \left|\boldsymbol{\psi}_2^R\right\rangle &= \begin{pmatrix} -\frac{j}{\sqrt{2}}\sqrt{\frac{m_{eff}\omega^2 - k_f}{ka^2}} \\ \frac{1}{\sqrt{2}} \end{pmatrix} & \left\langle \boldsymbol{\psi}_2^L \right| &= \begin{pmatrix} -\frac{1}{j\sqrt{2}}\sqrt{\frac{ka^2}{m_{eff}\omega^2 - k_f}} & \frac{1}{\sqrt{2}} \end{pmatrix} \end{aligned} \tag{9}$$

Note that the bra-ket notation $\langle \boldsymbol{a}|\ \boldsymbol{b}\rangle$ is equivalent to $\boldsymbol{a}^\dagger \cdot \boldsymbol{b}$, being $\boldsymbol{a}$ and $\boldsymbol{b}$ column vectors and $(\cdot)^\dagger$ the Hermitian conjugate. While $\langle \boldsymbol{a}|\, A\, |\boldsymbol{b}\rangle$ is equivalent to $\boldsymbol{a}^\dagger A \boldsymbol{b}$. Also, the mathematical steps to get to Eq. (8) are reported in Appendix and discussed in detail.

We are now ready to assess adiabaticity of graded metamaterials and perform numerical simulations.

4. Numerical results

To support the above discussion, we produce numerical simulations, where three different modulation steepnesses v_m are employed, or equivalently, the number of elements N is chosen in order for the resonators to operate between $\omega_{r,i}$ and $\omega_{r,f}$. The values for N are chosen across the adiabatic limit, in an attempt to capture how the steepness of the grading v_m affects the scattering process that takes place within the material. By way of Eqs. (7)–(9) we get an expression for the adiabatic limit:

$$\left| m_{eff,x} \frac{\omega^2}{8} \sqrt{\frac{ka^2}{\left(-k_f + m_{eff}\omega^2\right)^3}} \right| << 1, \tag{10}$$

which is a function of space, the steepness of the grading (included in the term $m_{eff,x}$), and the excitation frequency ω (included in the terms $m_{eff,x}$ and m_{eff}). In other words, different points along the MEMS chain are associated with different conditions for adiabaticity. We remark that also k_f plays a role in Eq. (10), which has a minimal influence if the excitation frequency is close to resonance, consistently with the analysis reported in Fig. 3(b) and since $m_{eff} \to \infty$ if $\omega \to \omega_r$.

To illustrate the concept of adiabatic limit, the expression in Eq. (10) is graphically represented in Fig. 4(a) upon varying the number of resonators N, evaluated for an incident wave at frequency $\omega_{IN} = 0.88\,\omega_{r,f}$, and plotted along the normalized position x/L_m, being $L_m = Na$ the total length of the grading region. $\omega_{IN} = 0.88\,\omega_{r,f}$ is chosen sufficiently below the gap. The domains defined through Eq. (10), and displayed in Fig. 4(a), are obtained by way of a thresholding process that saturates to 0.01, which is considered a reasonable choice to delineate a border between adiabatic and nonadiabatic transformations.

The black color delineates the regions in which the transformation occurs adiabatically, while within the white regions the process is nonadiabatic and, hence, generates scattering. Note that in the figure, three horizontal lines are marked to show the values employed in the numerical simulations, hereafter discussed. The corresponding three spatial evolution of the amplitude defined Eq. (10) are reported in Fig. 4(b). As expected from prior works on the topic, we observe that the critical point occurs at spatial regions where the resonant frequency of the grading approaches the frequency of the impinging wave. In the limit $\omega_r \to \omega_{IN}$, the expression into Eq. (10) goes to infinity and, as expected, adiabaticity can be met only with infinitely long lattices.

Now, to better illustrate the role of the grading steepnesses on the phenomenon, a large domain with $N_{tot} = 280$ elements is employed. The first 40 cells have a constant resonant frequency $\omega_r = \omega_{r,i}$, which is regarded as the input domain, where the wave is generated. A second domain with variable size N embodies the grading, whereby the resonator's frequency is varied between $\omega_{r,i}$ to $\omega_{r,f}$ through a finite number N of MEMS elements. The grading is then connected to a third domain, where the resonators exhibit a constant frequency equal to $\omega_{r,f}$. And finally, 80 elements are added to provide absorbing boundaries and, hence, prevent undesired reflections.

The wavefields are generated through an input force with a central frequency of ω_{IN} and a number of periods $n = 20$, to provide narrowband spectrum tone burst excitation sufficiently below the gap

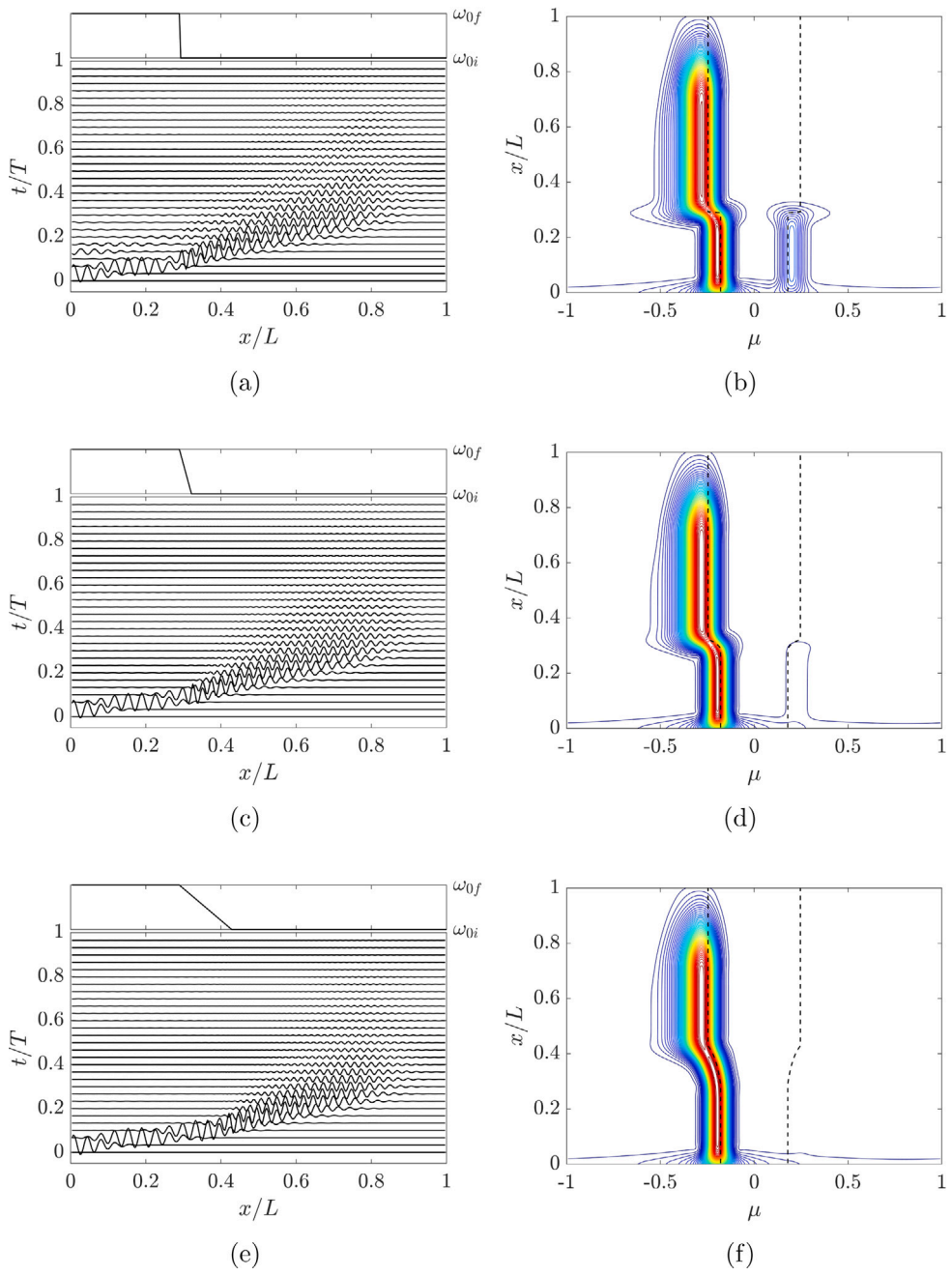

Fig. 5. (a,c,e) wavefields $u(x,t)_{,x}$ obtained with $N = 2$, $N = 10$, $N = 40$, where N is the number of elements within the grading. The corresponding values for ω_r are displayed atop the wavefield. (b,d,f) Corresponding spectrograms, where the expected evolution of the wavenumber is marked with dashed lines.

(otherwise an infinitely long system would have been needed to explore adiabaticity). Figs. 5(a), 5(c), and 5(e) illustrate the results in terms of deformations of the lattice $u(x,t)_{,x}$ for the three aforementioned values for N. The wavefield is later windowed with a moving Gaussian function $G(x,x_0) = \mathrm{e}^{-\frac{(x-x_0)^2}{2c^2}}$, where the moving parameter is $x_0 \in [0, N_{tot}a]$ and c is a parameter that determines the width of the Gaussian function. The windowed wavefield is Fourier transformed in reciprocal space $\hat{u}(\mu,\omega,x_0)_{,x}$ and reduced to $\hat{u}(\mu,x_0)_{,x}$ by taking the L^2 norm along the frequency dimension. This allows mapping the wavenumber content into spectrograms, as shown in 5(b), 5(d), and 5(f). In the spectrograms, negative wavenumbers denote the left-to-right traveling waves, while positive values represent a wave that is scattered back and propagates toward the opposite direction. Interestingly, we observe a transition that takes place when different values of N are considered, whereby the energy, initially injected before the grading, is partially reflected as a back-scattered wave (Figs. 5(a–b)). The transmitted energy is instead wavenumber-transformed and slowed down, which is the blueprint of the rainbow effect. When the number of elements is increased to $N = 10$ (Figs. 5(c–d)), the amount of reflection is decreased and more energy is converted to exhibit a different wavenumber content. For a long array of elements made of $N = 40$ unit cells (Figs. 5(e–f)), the process can be considered adiabatic and the amount of scattering is negligible.

5. Conclusions

In this paper, we have used the adiabatic theorem to investigate the dynamics of graded metamaterials in the context of MEMS spring–mass chain. In analogy with prior works on time-dependent lattices (Santini and Riva, 2023), the link between the grading steepness and the rainbow effect has been revealed, providing a quantitative condition for the

wavenumber transformation to occur without scattering. When such a condition is satisfied, there is the formation of arbitrarily slow waves emerging from an adiabatic variation of the resonators' frequency in space, which are functional for next-generation applications, such as energy harvesting, communication, and signal processing. This work also suggests new ways to design spatially graded metamaterials at the micro-scale.

Declaration of competing interest

The authors declare that they have no known competing financial interests or personal relationships that could have appeared to influence the work reported in this paper.

Data availability

Data will be made available on request.

Acknowledgments

The support of the H2020 FET-proactive Metamaterial Enabled Vibration Energy Harvesting (MetaVEH) project under Grant Agreement No. 952039 is acknowledged.

This article is dedicated to Prof. Viggo Tvergaard on the occasion of his 80th birthday.

Appendix. The adiabatic theorem for propagating waves

The derivation of the adiabaticity condition between state 1 and 2 described through Eq. (8) is herein reported. The discussion starts with the equation of motion (7) with implied frequency dependence. A solution is expressed in exponential form $|\boldsymbol{\Psi}\rangle = |\boldsymbol{\psi}_n^R\rangle \, \mathrm{e}^{j\kappa_n x}$, which results in a space-dependent instantaneous eigenvalue problem $H(x,\omega)\,|\boldsymbol{\psi}_n^R\rangle = j\kappa_n |\boldsymbol{\psi}_n^R\rangle$. The space-varying eigenvalue $j\kappa_n(x)$ and relative right eigenvector $|\boldsymbol{\psi}_n^R\rangle(x)$ define the dispersion branches for any incident frequency ω. Here $n = [1,2]$, which *de facto* represents two counter-propagating waves with opposite wavenumbers $\kappa_1 = -\kappa_2$.

After time modulation takes place, the solution consists of the linear combination of all available wave modes $|\boldsymbol{\Psi}\rangle = \sum_n c_n(x)\,|\boldsymbol{\psi}_n^R\rangle(x)\,\mathrm{e}^{j\theta_n}$, where $\theta_n = \int_0^x \kappa_n(\xi)\,d\xi$ is the geometric phase of the wave and c_n is the space-dependent participation factor the nth wave mode. Plugging this Ansatz into Eq. (8) and after a few mathematical manipulations (Santini and Riva, 2023) we get to a space-dependent differential equation for the coefficients $c_r(x)$, with $r = [1,2]$:

$$c_{r,x} = -\langle \boldsymbol{\psi}_r^L \mid \boldsymbol{\psi}_r^R \rangle \, c_r - \sum_{n\neq r} \frac{\langle \boldsymbol{\psi}_r^L |\, H_{,x}\, |\boldsymbol{\psi}_n^R\rangle}{j\left(\kappa_n - \kappa_r\right)} c_n \mathrm{e}^{j(\theta_n-\theta_r)} \tag{A.1}$$

Suppose now the energy is initially injected in the right propagating wave, i.e., $c_1(0) = 1$ and $c_2(0) = 0$. If the integral of the coupling term in Eq. (A.1) is small, the energy cannot leak toward other states:

$$\int_0^x \sum_{n\neq r} \frac{\langle \boldsymbol{\psi}_r^L |\, H_{,x}\, |\boldsymbol{\psi}_n^R\rangle}{j\left(\kappa_n - \kappa_r\right)} c_n \mathrm{e}^{j(\theta_n-\theta_r)} d\xi = -\sum_{n\neq r} \frac{\langle \boldsymbol{\psi}_r^L |\, H_{,x}\, |\boldsymbol{\psi}_n^R\rangle}{\left(\kappa_n - \kappa_r\right)^2} c_n \mathrm{e}^{j(\theta_n-\theta_r)} \Bigg|_0^x + \int_0^x \frac{d}{d\xi}\left(\sum_{n\neq r} \frac{\langle \boldsymbol{\psi}_r^L |\, H_{,x}\, |\boldsymbol{\psi}_n^R\rangle}{\left(\kappa_n - \kappa_r\right)^2} c_n \mathrm{e}^{j(\theta_n-\theta_r)} \right) \tag{A.2}$$

where the integral term on the right-hand side is negligible since further integration involves higher-order powers for the term at the denominator $\left(\kappa_n - \kappa_r\right)$ (Santini and Riva, 2023). We retain the first term and finally get to:

$$\left| \frac{\langle \boldsymbol{\psi}_r^L |\, H_{,x}\, |\boldsymbol{\psi}_n^R\rangle}{\left(\kappa_r - \kappa_n\right)^2} \right| \ll 1 \tag{A.3}$$

which represents the limiting condition in order for the energy, initially injected into the rth wave mode, not to leak to the nth state.

References

Alan, S., Allam, A., Erturk, A., 2019. Programmable mode conversion and bandgap formation for surface acoustic waves using piezoelectric metamaterials. Appl. Phys. Lett. 115 (9), 093502.

Alshaqaq, M., Sugino, C., Erturk, A., 2022. Programmable rainbow trapping and bandgap enhancement via spatial group-velocity tailoring in elastic metamaterials. Phys. Rev. A 17, L021003.

Antonakakis, T., Craster, R.V., Guenneau, S., 2013. Asymptotics for metamaterials and photonic crystals. Proc. R. Soc. A 469, 1–20.

Cha, J., Kim, K., Daraio, C., 2018. Experimental realization of on-chip topological nanoelectromechanical metamaterial. Nature 564, 229–233.

Chaplain, G.J., De Ponti, J.M., Aguzzi, G., Colombi, A., Craster, R.V., 2020a. Topological rainbow trapping for elastic energy harvesting in graded Su-Schrieffer-Heeger systems. Phys. Rev. A 14 (5), 054035.

Chaplain, G.J., De Ponti, J.M., Colombi, A., Fuentes-Dominguez, R., Dryburg, P., Pieris, D., Smith, R.J., Clare, A., Clark, M., Craster, R.V., 2020b. Tailored elastic surface to body wave Umklapp conversion. Nature Commun. 11 (3267).

Chaplain, G., Pajer, D., De Ponti, J.M., Craster, R., 2020c. Delineating rainbow reflection and trapping with applications for energy harvesting. New J. Phys. 22 (6), 063024.

Colombi, A., Colquitt, D., Roux, P., Guenneau, S., Craster, R., 2016a. A seismic metamaterial: The resonant metawedge. Sci. Rep. 6, 27717.

Colombi, A., Guenneau, S., Roux, P., Craster, R., 2016b. Transformation seismology: composite soil lenses for steering surface elastic Rayleigh waves. Sci. Rep. 6, 1–9.

Corigliano, A., Ardito, R., Comi, C., Frangi, A., Ghisi, A., Mariani, S., 2017. Mechanics of Microsystems. John Wiley '&' Sons Inc.

De Ponti, J.M., 2021. Graded Elastic Metamaterials for Energy Harvesting. Springer International Publishing.

De Ponti, J.M., 2022. Autonomous wireless sensors via graded elastic metamaterials. In: Antonelli, M., Della Vecchia, G. (Eds.), Civil and Environmental Engineering for the Sustainable Development Goals: Emerging Issues. Springer International Publishing, Cham, pp. 55–66.

De Ponti, J.M., Colombi, A., Ardito, R., Braghin, F., Corigliano, A., Craster, R.V., 2019. Graded elastic metasurface for enhanced energy harvesting. New J. Phys. 22, 013013.

De Ponti, J.M., Colombi, A., Riva, E., Ardito, R., Braghin, F., Corigliano, A., Craster, R., 2020. Experimental investigation of amplification, via a mechanical delay-line, in a rainbow-based metamaterial for energy harvesting. Appl. Phys. Lett. 117 (143902), 1–6.

De Ponti, J.M., Iorio, L., Chaplain, G.J., Corigliano, A., Craster, R.V., Ardito, R., 2023. Tailored topological edge waves via chiral hierarchical metamaterials. Phys. Rev. A 19 (3), 034079.

De Ponti, J.M., Iorio, L., Riva, E., Ardito, R., Braghin, F., Corigliano, A., 2021a. Selective mode conversion and rainbow trapping via graded elastic waveguides. Phys. Rev. A 16, 034028.

De Ponti, J.M., Iorio, L., Riva, E., Braghin, F., Corigliano, A., Ardito, R., 2021b. Enhanced energy harvesting of flexural waves in elastic beams by bending mode of graded resonators. Front. Mater. 8, 1–7.

Deng, B., Zanaty, M., Forte, A.E., Bertoldi, K., 2022. Topological solitons make metamaterials crawl. Phys. Rev. A 17, 014004.

Dubček, T., Moreno-Garcia, D., Haag, T., Thomsen, H.R., Becker, T.S., Bärlocher, C., Andersson, F., Huber, S.D., van Manen, D.-J., Villanueva, L.G., et al., 2021. Binary classification of spoken words with passive elastic metastructures. arXiv preprint arXiv:2111.08503.

Grinberg, I.H., Lin, M., Harris, C., Benalcazar, W.A., Peterson, C.W., Hughes, T.L., Bahl, G., 2020. Robust temporal pumping in a magneto-mechanical topological insulator. Nat. Commun. 11 (1), 974.

Huber, S.D., 2016. Topological mechanics. Nat. Phys. 12, 621—623.

Marconi, J., Quadrelli, D.E., Braghin, F., 2023. Non-reciprocal MEMS periodic structure. Actuators 12, 161.

Marconi, J., Riva, E., Di Ronco, M., Cazzulani, G., Braghin, F., Ruzzene, M., 2020. Experimental observation of nonreciprocal band gaps in a space-time-modulated beam using a shunted piezoelectric array. Phys. Rev. A 13 (3), 031001.

Milton, G.W., Willis, J.R., 2007. On modifications of Newton's second law and linear continuum elastodynamics. Proc. R. Soc. Lond. Ser. A Math. Phys. Eng. Sci. 463, 855–880.

Miniaci, M., Pal, R., Morvan, B., Ruzzene, M., 2018. Experimental observation of topologically protected helical edge modes in patterned elastic plates. Phys. Rev. X 8 (3), 031074.

Moore, J.E., 2010. The birth of topological insulators. Nature 464, 194–198.

Mousavi, S., Khanikaev, A., Wang, Z., 2015. Topologically protected elastic waves in phononic metamaterials. Nature Commun. 6, 1–7.

Palermo, A., Celli, P., Yousefzadeh, B., Daraio, C., Marzani, A., 2020. Surface wave non-reciprocity via time-modulated metamaterials. J. Mech. Phys. Solids 145, 104181.

Palermo, A., Krödel, S., Marzani, A., Daraio, C., 2016. Engineered metabarrier as shield from seismic surface waves. Sci. Rep. 6 (1), 1–10.

Riva, E., Castaldini, G., Braghin, F., 2021. Adiabatic edge-to-edge transformations in time-modulated elastic lattices and non-hermitian shortcuts. New J. Phys. 23 (9), 093008.

Riva, E., Quadrelli, D., Cazzulani, G., Braghin, F., 2018. Tunable in-plane topologically protected edge waves in continuum Kagome lattices. J. Appl. Phys. 124 (16), 164903.

Riva, E., Rosa, M.I., Ruzzene, M., 2020. Edge states and topological pumping in stiffness-modulated elastic plates. Phys. Rev. B 101 (9), 094307.

Santini, J., Riva, E., 2023. Elastic temporal waveguiding. New J. Phys. 25 (1), 013031.

Santini, J., Sugino, C., Riva, E., Erturk, A., 2022. Harnessing rainbow trapping via hybrid electromechanical metastructures for enhanced energy harvesting and vibration attenuation. J. Appl. Phys. 132 (6), 064903.

Sridhar, A., Kouznetsova, V., Geers, M.G.D., 2016. Homogenization of locally resonant acoustic metamaterials towards an emergent enriched continuum. Comput. Mech. 57, 423–435.

Tol, S., Degertekin, F.L., Erturk, A., 2017. Phononic crystal luneburg lens for omnidirectional elastic wave focusing and energy harvesting. Appl. Phys. Lett. 111 (1), 013503.

Tsakmakidis, K.L., Boardman, A.D., Hess, O., 2007. 'Trapped rainbow' storage of light in metamaterials. Nature 450 (7168), 397–401.

Wang, P., Lu, L., Bertoldi, K., 2015. Topological phononic crystals with one-way elastic edge waves. Phys. Rev. Lett. 115 (10), 104302.

Xia, Y., Riva, E., Rosa, M.I., Cazzulani, G., Erturk, A., Braghin, F., Ruzzene, M., 2021. Experimental observation of temporal pumping in electromechanical waveguides. Phys. Rev. Lett. 126 (9), 095501.

Yan, W., Gao, Y., 2023. Steering of flexural wave propagation in tunable magnetorheological elastomers metasurface by modulating magnetic field. Int. J. Mech. Sci. 237, 107793.

Zhao, B., Thomsen, H.R., De Ponti, J.M., Riva, E., Van Damme, B., Bergamini, A., Chatzi, E., Colombi, A., 2022. A graded metamaterial for broadband and high-capability piezoelectric energy harvesting. Energy Convers. Manage. 269, 116056.